Molecular Pharmacology Fast Forward. Published on September 26, 2014 as DOI: 10.1124/mol.114.095869
This article has not been copyedited and formatted. The final version may differ from this version.

Exon 3 splicing and mutagenesis identify residues influencing cell surface density of heterologously-expressed silkworm (*Bombyx mori*) glutamate-gated chloride channels

Shogo Furutani, Makoto Ihara, Yuri Nishino, Miki Akamatsu, Andrew K. Jones, David B. Sattelle and Kazuhiko Matsuda

Department of Applied Biological Chemistry, Faculty of Agriculture, Kinki University, 3327-204 Nakamachi Nara, 631-8505, Japan (S.F., M.I., K.M.)

Graduate School of Life Science, University of Hyogo, 3-2-1, Koto, Kamigori-cho, Ako-gun, Hyogo 678-1297, Japan (Y.N.)

Graduate School of Agriculture, Kyoto University, Sakyo-Ku, Kyoto 606-8502, Japan (M.A.)

Department of Biological and Medical Sciences, Faculty of Health and Life Sciences, Oxford Brookes University, Gipsy Lane, Oxford, OX3 0BP, United Kingdom (A.K.J.)

The Wolfson Institute for Biomedical Research, Department of Medicine, Cruciform Building, University College London, Gower Street, London, WC1E 6BT, United Kingdom (D.B.S.)

Primary laboratory origin: Department of Applied Biological Chemistry, Faculty of Agriculture, Kinki University

Molecular Pharmacology Fast Forward. Published on September 26, 2014 as DOI: 10.1124/mol.114.095869
This article has not been copyedited and formatted. The final version may differ from this version.

Running title: Structural features influencing GluCl numbers in membranes

To whom correspondence should be addressed: Kazuhiko Matsuda
Department of Applied Biological Chemistry, Faculty of Agriculture, Kinki University
3327-204 Nakamachi, Nara 631-8505, Japan
Tel. +81-742-437153; Fax: +81-742-431445; E-mail: kmatsuda@nara.kindai.ac.jp

Number of text pages	35
Number of tables	1
Number of figures	4
Number of references	43
Number of words in Abstract	244 words
Number of words in Introduction	706 words
Number of words in Discussion	1624 words

Abbreviations: BmGluCl, *Bombyx mori* glutamate-gated chloride channel; HEPES, 4-(2-hydroxyethyl)piperazine-1-ethanesulfonic acid; IVM, ivermectin; PDB, Protein Data Bank; SOS, standard oocyte saline

Molecular Pharmacology Fast Forward. Published on September 26, 2014 as DOI: 10.1124/mol.114.095869
This article has not been copyedited and formatted. The final version may differ from this version.

Abstract

Glutamate-gated chloride channels (GluCls) mediate fast inhibitory neurotransmission in invertebrate nervous systems. I Insect GluCls show alternative splicing and to determine its impact on channel function and pharmacology we isolated GluCl cDNAs from larvae of the silkworm (*Bombyx mori*). We show that 6 BmGluCl variants are generated by splicing in exons 3 and 9 and that exons 3b and 3c are common in the brain and third thoracic ganglion. When expressed in *Xenopus laevis* oocytes, the three functional exon 3 variants (3a, b, c) all had similar EC_{50} values for L-glutamate and ivermectin (IVM); however, I_{max} (the maximum L-glutamate- and IVM-induced response of the channels at saturating concentrations) differed strikingly between variants, with the 3c variant showing the largest L-glutamate- and IVM-induced response. By contrast, a partial deletion detected in exon 9 had a much smaller impact on L-glutamate and IVM actions. Binding assays using [^{3}H]IVM indicate that diversity in IVM responses among the GluCl variants are mainly due to the impact on channel assembly, altering receptor cell surface numbers. GluCl variants expressed in HEK293 cells show that structural differences influenced B_{max} but not K_d values of [^{3}H]IVM. Domain swapping and site-directed mutagenesis identified 4 amino acids in exon 3c as hot spots determining the highest amplitude of the L-glutamate and IVM responses. Modeling the GluCl 3a and 3c variants suggested that 3 of the 4 amino acids contribute to inter-subunit contacts, while the other interacts with the TM2-TM3 linker, influencing the receptor response.

Molecular Pharmacology Fast Forward. Published on September 26, 2014 as DOI: 10.1124/mol.114.095869
This article has not been copyedited and formatted. The final version may differ from this version.

Introduction

The di-cysteine loop ligand-gated ion channels (cys-loop LGICs) permeable to chloride play an important role in inhibitory neurotransmission in both vertebrates and invertebrates. Five subunits, each consisting of four transmembrane (TM) domains, assemble to form a chloride-ion permeable channel that opens in response to the binding of neurotransmitters. As the equilibrium potential for chloride is close to the resting membrane potential, activation of this type of channel counteracts excitatory neurotransmitter-induced membrane depolarization. γ-Aminobutyric acid (GABA)-gated chloride channels are widely expressed in the nervous systems of arthropods and nematodes as well as in higher animals (Buckingham et al., 2005). Whereas glycine-gated chloride channels are also present in vertebrates, chloride channels gated by L-glutamate (GluCls) (Wolstenholme, 2012), dopamine (DACls) (Ringstad et al., 2009), tyramine (TyrCls) (Ringstad et al., 2009), histamine (HisCls) (Gengs et al., 2002; Gisselmann et al., 2002; Hardie, 1989; Pantazis et al., 2008; Zheng et al., 2002) and acetylcholine (AChCls) (Putrenko et al., 2005) are found only in invertebrates. Such channels are important candidate targets for the development of anthelmintics and insecticides (Raymond and Sattelle, 2002; Wolstenholme, 1997; Wolstenholme et al., 2007; Wolstenholme and Rogers, 2005).

Glutamate-gated chloride channels (GluCls) were first discovered in electrophysiological studies on locust muscle. When L-glutamate was applied, a biphasic (depolarizing and hyperpolarizing) change in muscle membrane potential was observed; the hyperpolarizing phase was the result of enhanced chloride ion permeability (Cull-Candy, 1976). L-Glutamate-enhanced chloride permeability was also observed in the fast coxal depressor motor neurone of the American cockroach (Wafford and Sattelle, 1986). The molecular components of a GluCl were elucidated by the isolation of the *glucl*-α and β genes from the nematode *Caenorhabditis elegans* as the target of an antihelmintic drug ivermectin (IVM)

Molecular Pharmacology Fast Forward. Published on September 26, 2014 as DOI: 10.1124/mol.114.095869
This article has not been copyedited and formatted. The final version may differ from this version.

(Cully et al., 1994). When expressed alone in *Xenopus laevis* oocytes, the α-subunit was activated by IVM but not by L-glutamate, whereas the reverse was the case for the β-subunit (Cully et al., 1994). The pharmacology of the recombinant nematode GluCl most resembled that of the native receptor when both α and β subunits were co-expressed in oocytes. Subsequently, third and fourth genes were shown to contribute to IVM sensitivity (Wolstenholme and Rogers, 2005) and six *C. elegans* GluCl subunits are now known (Jones and Sattelle, 2008). In contrast, a single GluCl subunit was isolated from *Drosophila melanogaster*, which generates an ivermectin-sensitive channel when expressed in *X. laevis* oocytes (Cully et al., 1996). Subsequent analysis of genome sequences have shown that several insect species possess only a single *glucl* gene (Jones and Sattelle, 2006; Jones and Sattelle, 2007; Jones et al., 2010).

Even a single gene can yield diverse receptor subtypes. For example, the gene encoding the *Drosophila* GABA-gated chloride channel (RDL: resistant to dieldrin), exhibits alternative splicing at exons 3 and 6, generating multiple products (ffrench-Constant and Rocheleau, 1993). Splicing and A-to-I pre-mRNA editing adds to diversity, resulting in functional receptors with divergent affinity for GABA measured by differences in EC_{50} (Jones et al., 2009). These transcriptional modifications vary depending on the stage of development. Notably, the RNA editing occurs more frequently in adults than in embryonic and larval stages (Jones et al., 2009). Recently a detailed characterization of the pharmacology of the most abundantly expressed splice/edit isoform of *Drosophila* RDL has been described (Lees et al 2014).

In the case of GluCls, splice variants have been found in *Drosophila* larvae (Semenov and Pak, 1999), where exon 3 is alternatively spliced. This splicing is conserved in diverse insect species (Jones et al., 2009). However, little is known about the role of GluCl splicing diversity in the nervous system. The silkworm (*Bombyx mori*) genome of about 475 Mb has been fully sequenced (Mita et al., 2004; Xia et al., 2004). Its large larval size, compared to other model

Molecular Pharmacology Fast Forward. Published on September 26, 2014 as DOI: 10.1124/mol.114.095869
This article has not been copyedited and formatted. The final version may differ from this version.

insects, permits the isolation of various organs. Also, the silkworm is evolutionally close to lepidopteran insect pests, offering a platform for screening candidate pesticides. Therefore, we have isolated from the silkworm nervous system cDNAs transcribed from the single GluCl (BmGluCl) gene. We show that although splicing-induced variations of GluCls do not impact on the EC_{50} values for L-glutamate and IVM, they do profoundly influence the peak (I_{max}) GluCl response to both ligands and that four amino acids play key roles in determining the cell surface numbers of GluCl.

Materials and Methods

Chemicals

L-Glutamate and IVM were purchased from Sigma-Aldrich (MO, USA) and used without further purification.

Cloning of GluCl cDNAs and their sequences

Whole brains and the third thoracic ganglia from the last instar larvae of *B. mori* (p50, 'Daizo' strain) were isolated and homogenized separately with TRIzol reagent (Life Technologies, Carlsbad, CA, USA) to extract RNAs, which were further treated with TURBO DNase (Life Technologies). To obtain the GluCl 5'end, 1st round PCR was carried out with KOD -Plus- DNA polymerase (Toyobo, Osaka, Japan) and a pair of primers (forward, CGACTGGAGCACGAGGACACTGA; reverse, GTTCCGTTGATGCCTGACGG) using first strand cDNA prepared by GeneRacer kit (Life Technologies), according to the following PCR cycles: 94˚C for 2 min followed by 30 cycles of 94˚C for 15 s, 56˚C for 30 s and 68˚C for 2 min. An aliquot (1 μl) of this reaction was used for 2nd round PCR by KOD -Plus- DNA polymerase using primers (forward, GGACACTGACATGGACTGAAGGAGTA; reverse, GGTCCAAGATCTGCTTCTCC) with the same cycle reaction as used in the 1st round PCR.

Molecular Pharmacology Fast Forward. Published on September 26, 2014 as DOI: 10.1124/mol.114.095869
This article has not been copyedited and formatted. The final version may differ from this version.

The PCR product was treated with Taq DNA polymerase (Takara Bio, Shiga, Japan) at 72˚C for 30 min, gel purified and cloned into either pGEM-T (Promega, WI, USA), or TOPO cloning vector (Life Technologies).

The 3' cDNA end was amplified by nested PCR using KOD -Plus- DNA polymerase, a pair of primers [1st round PCR (forward, TGGACACTAAGATGCGGCAGTGC; reverse, GCTGTCAACGATACGCTACGTAACG); 2nd round PCR (forward, TGTCCAAGTTTCCCACGCGCTCC; reverse, CGCTACGTAACGGCATGACAGTG)] and the first strand cDNA prepared with the GeneRacer kit according to the reaction cycle described above. In some cases, the 3' end was determined using SMARTer RACE cDNA Amplification kit (Clontech Laboratories, CA, USA).

Full length cDNAs of BmGluCls were amplified by KOD -Plus- DNA polymerase using forward (CGGGGTACCATGGAATTCCCTCGGCGGCCATGT) and reverse (CAGGGATCCTCACCAGTAAGCCAAATTGAAAATG or GCGGGATCCTCACTTCTCTTCCTCCTCGTCGCGAAACAAATATGTTG for Type I and Type II BmGluCls, respectively) primers according to the following PCR cycle: 94˚C for 2 min followed by 30 cycles of 94˚C for 15 s, 56˚C for 30 s and 68˚C for 2 min. Amplified full length cDNA of BmGluCls were gel-purified, digested with *Kpn*I and *Bam*HI and cloned into the same restriction sites of pcDNA3.1 (+) vector (Life Technologies). The entire cDNA sequence was determined using a 3100 Genetic Analyzer (Life Technologies).

Real time PCR analysis

The mRNAs for BmGluCl were quantified by real time PCR using a 7500 Real Time PCR System (Life Technologies) with exon-specific primers (exon 3a, exon 3b, exon 3c, exon 3 deleted (3Δ), exon 9, exon 9 partially deleted (9pΔ, see Supplemental Table 1). The PCR was

Molecular Pharmacology Fast Forward. Published on September 26, 2014 as DOI: 10.1124/mol.114.095869
This article has not been copyedited and formatted. The final version may differ from this version.

conducted using 500 ng of total RNA and the PrimeScript™ RT Reagent Kit (Perfect Real Time) (Takara Bio) together with FastStart Universal SYBR Green Master (Rox) (F. Hoffmann-La Roche, Basel, Switzerland) according to following PCR cycle: denaturing at 94˚C for 2 min followed by a cycle reaction up to 40 cycles of 94˚C for 15 s, 60˚C for 30 s and 68˚C for 2 min. *B. mori actin* A3 gene (GenBank accession no: X04507) was amplified as reference by the same reaction protocol using forward (GCGCGGCTACTCGTTCACTACC) and reverse (GGATGTCCACGTCGCACTTCA) primers to obtain a ΔCt value (=Ct (target gene)-Ct (actin)). Relative mRNA expression levels were compared by normalizing the ΔCt value for the variant to that for exon 3a sequence.

cRNA preparation for functional expressions of BmGluCl variants in *Xenopus laevis* oocytes

The pcDNA3.1 vector carrying a BmGluCl cDNA was linearized with *Bam*HI and used as a template for transcription of cRNA. The cRNA was prepared using the mMESSAGE mMACHINE T7 kit (Life Technologies) together with the linearized cDNA and was dissolved in RNase-free water at a concentration of 1 mg ml^{-1} and stored at -80 °C until use.

Functional expression of BmGluCls in *Xenopus laevis* oocytes

The ovary of *Xenopus laevis* was removed from anesthetized *X. laevis* according to the U. K. Animals (Scientific Procedures) Act, 1986. The oocytes were treated with 2.0 mg ml^{-1} collagenase (Type IA, Sigma-Aldrich) in the Ca^{2+}-free standard oocyte saline (SOS) of the following composition: 100 mM NaCl, 2 mM KCl, 1 mM $MgCl_2$ and 5 mM 4-(2-hydroxyethyl)-1-piperazineethanesulfonic acid (HEPES) 5.0 (pH 7.6), and then transferred into SOS consisting of 100 mM NaCl, 2 mM KCl, 1.8 mM $CaCl_2$, 1 mM $MgCl_2$ and 5 mM

Molecular Pharmacology Fast Forward. Published on September 26, 2014 as DOI: 10.1124/mol.114.095869
This article has not been copyedited and formatted. The final version may differ from this version.

HEPES 5.0 (pH 7.6). Oocytes at stage V or VI of development were defoliculated manually using a pair of fine forceps. Then each oocyte was injected with 50 nl of the cRNA solution of BmGluCl and incubated at 16°C in SOS supplemented with penicillin (100 units ml^{-1}), streptomycin (100 μg ml^{-1}), gentamycin (20 μg ml^{-1}) and 2.5 mM sodium pyruvate. Electrophysiology was conducted one day after cRNA injection.

Voltage-clamp electrophysiology

The recording of the L-glutamate-induced currents in oocytes under voltage-clamp was carried out at room temperature (18 – 23°C). The *X. laevis* oocytes were secured in a recording chamber that was continuously perfused with SOS at a flow rate of 7 – 10 ml min^{-1}. Membrane currents were recorded with a GENECLAMP 500B amplifier (Molecular Devices, CA, USA) at a holding potential of -80 mV. The electrodes were filled with 2 M KCl and had a resistance of 1 – 5 MΩ when measured in SOS. Signals were digitized by a Digidata 1200 data acquisition system (Molecular Devices) and recorded using Clampex 8 (Molecular Devices). L-Glutamate was directly dissolved in SOS. In the case of IVM, each test solution was prepared by diluting the 10 mM stock solution in dimethyl sulfoxide with SOS. Test solutions were applied to oocytes for 3 – 5 s, with an interval of 3 min between applications. However, it was difficult to completely remove IVM when tested at concentrations above 1 μM. In such cases, only a single exposure to IVM was applied per oocyte.

Analysis of electrophysiological data

Membrane currents were analyzed using Clampfit 9 (Molecular Devices). The concentration-response curves for L-glultamate and IVM of BmGluCls were fitted with the following equation, using Prism 4 software (GraphPad Software, CA, USA):

Molecular Pharmacology Fast Forward. Published on September 26, 2014 as DOI: 10.1124/mol.114.095869
This article has not been copyedited and formatted. The final version may differ from this version.

$$Y = \frac{Imax}{1+10^{(\log EC_{50}-[A])\cdot n_H}} \quad (1)$$

where Y is the normalized response, I_{max} is the peak current amplitude (μA) of the L-glutamate-induced response, EC_{50} (M) is the half maximal effective concentration, [A] is the logarithm of the concentration of L-glutamate (M) and n_H is the Hill coefficient.

[^{3}H]IVM binding on oocyte membrane proteins

One hundred *Xenopus* oocytes expressing each GluCl variant were homogenized in homogenizing buffer (10 mM HEPES, 250 mM sucrose, 1 mM EGTA, and 2 mM $MgCl_2$, pH 7.4) supplemented with complete protease inhibitor cocktail (F. Hoffmann-La Roche) on ice and the homogenates were centrifuged at 500 x *g*. The supernatant was centrifuged at 25,000 x g to obtain the membrane fraction, which was suspended in homogenizing buffer and centrifuged again at 25,000 x g. The resultant membrane fraction was suspended in 50 mM HEPES buffer (pH 7.4) and the protein concentration was determined using the Bradford method.

[^{3}H]IVM (50 Ci/mmol) was purchased from American Radiolabeled Chemicals, Inc. (Saint Louis, MO, USA). Membrane homogenates (20 μg protein) of the *Xenopus* oocytes were incubated with 1 nM [^{3}H]IVM in 0.5 mL of 50 mM HEPES buffer (pH 7.4) containing 0.02% Triton X-100 at 22°C for 60 min. Reaction mixtures for the determination of non-specific binding included 1 μM unlabelled IVM. After the incubation, reactions were terminated by rapid filtration through GF/B glass fiber filters (GE Healthcare Life Sciences, Uppsala, Sweden) presoaked in 50 mM HEPES buffer containing 0.1% polyethyleneimine using a Brandel M-24 cell harvester. Radioactivity on the filters was measured using an LSC-5100 liquid scintillation counter (Aloka, Japan). The K_d and B_{max} values of [^{3}H]IVM were determined by non-linear regression analysis using the Prism 4 software.

Molecular Pharmacology Fast Forward. Published on September 26, 2014 as DOI: 10.1124/mol.114.095869
This article has not been copyedited and formatted. The final version may differ from this version.

Expression of BmGluCls in HEK293 cells and [^{3}H]IVM binding

The HEK293 cells were transfected with the pcDNA 3.1 (+) vector containing the BmGluCl gene using Lipofectamine 2000 reagent (Life Technologies). Cells were collected 48 h after the transfection and homogenized in 50 mM HEPES buffer (pH 7.4) supplemented with complete protease inhibitor cocktail (F. Hoffmann-La Roche) on ice. The homogenates were centrifuged at 1,000 x g for 10 min. The supernatants were centrifuged at 25,000 x g for 30 min and the resulting pellets were suspended in 50 mM HEPES buffer (pH 7.4) for binding assays.

Binding assays on HEK293 cell membranes were performed as described for the oocyte membranes. Membrane homogenates (10 μg protein) were incubated with 0.075-9.6 nM [^{3}H]IVM in 50 mM HEPES buffer (pH 7.4) containing 0.02% Triton X-100 at 22°C for 60 min. Reactions were terminated by rapid filtration through Whatman GF/B glass fiber filters using a Brandel M-24 cell harvester. The filters were subsequently washed with cold distilled water containing 0.25% Triton X-100. Radioactivity on the filters was counted with the LSC-5100 liquid scintillation counter and the K_d and B_{max} values of [^{3}H]IVM were determined as described for BmGluCls expressed in *Xenopus* oocytes.

BmGluCl transcripts in the HEK293 cells were quantified by RT-PCR. Total RNA was isolated from HEK293 cells using RNeasy Plus Mini Kit (Qiagen, Hilden, Germany). The isolated RNA (2.5 μg) was reverse-transcribed using PrimeScript™ RT Reagent Kit (Takara Bio) and oligo $(dT)_{30}$ primer. A 250 bp *BmGluCl* gene fragment was amplified by PCR from single-stranded cDNA and primers (forward, TTCAGCTACTACCTCATCCA; reverse, GGGCGAACTCCAGTAGA). A 272 bp fragment of HEK293 cell β-actin cDNA (accession No. AB004047) was amplified as an internal control using primers (forward, ATCGTGATGGACTCCG; reverse, TCGTAGCTCTTCTCCAGG). PCR amplification was performed using KOD -Plus- (Toyobo, Osaka, Japan) as follows: an initial denaturation at 94°C

Molecular Pharmacology Fast Forward. Published on September 26, 2014 as DOI: 10.1124/mol.114.095869
This article has not been copyedited and formatted. The final version may differ from this version.

for 2 min, followed by 30 cycles at 98°C for 10 s, 57°C for 30 s and 68°C for 15 s.

Amino acid substitutions in exon 3a and exon 3c variants

In exons 3a and 3c, Block I nucleotide sequences were exchanged by overlap extension PCR with primers shown in Supplemental Table 2, while the Block II nucleotide sequences were mutated by inverse PCR with primers shown in Supplemental Table 3. DNA sequences of all the mutants were confirmed by DNA sequencing.

Modeling of BmGluCl variants

Homology models of BmGluCl exon 3a and exon 3c variants were constructed using the homology modeling software Protein Discovery Full Automatic Modeling System (PDFAMS Pro/Ligand&Complex; In-Silico Sciences, Tokyo, Japan) and the molecular modeling software package Sybyl (version 7.3; Tripos Associates, MO, USA). First, primary sequences of exon 3a and exon 3c variants of BmGluCl were aligned with the sequence of *C. elegans* GluCl α subunit and then the homodimer models complexed with L-glutamate and IVM were constructed based on the crystal structure of *C. elegans* GluCl α subunit with the two ligands (PDB code 3RIF) (Hibbs and Gouaux, 2011) by PDFAMS. The receptor model constructed in this way was energy-minimized for 5,000 iterations of conjugated gradients using the force field and partial charges of the molecular mechanics MMFF94 (Halgren, 1999a; Halgren, 1999b) using Sybyl. Finally, each model was represented graphically using Sybyl to identify structural features underpinning the characteristics of the variants. The PDB files of the homology models of BmGluCl exon 3a (BmGluCl3a.pdb) and 3c variants (BmGluCl3c.pdb) are provided in the supplemental data.

Molecular Pharmacology Fast Forward. Published on September 26, 2014 as DOI: 10.1124/mol.114.095869
This article has not been copyedited and formatted. The final version may differ from this version.

Results

Expression of BmGluCl variants in the silkworm

We amplified full-length BmGluCl cDNAs by RT-PCR from the silkworm larval brain and sequenced randomly-selected cloned cDNAs. The BmGluCl cDNAs encode peptide sequences possessing features common to cys-loop ligand-gated ion channels (Fig. 1B) including: an N-terminal signal peptide (first 24 residues); an extracellular N-terminal region containing the ligand-binding site and the di-cysteine loop (cys-loop); four transmembrane regions TM1–4 and a long intracellular TM3–TM4 linker. The BmGluCl gene consists of 11 exons, the last exon encoding the stop codon (Fig. 1A). Splice variants generated at exons 3 and 9 gave multiple cDNA products from the BmGluCl gene (Fig. 1B). Alternative splicing at exon 3, which encodes a part of the N- terminal ligand binding domain (LBD), generates three variants [Exons 3a (Accession number: KC342243), 3b (Accession number: KC342244) and 3c (Accession number: KC342245) while a fourth variant was observed, which completely lacks exon 3 [Exon 3Δ (Accession number: KC342246)]. Some BmGluCls containing either exon 3b or 3c possess an attenuated amino acid sequence after splicing at exon 9 (Fig. 1B). The exon 9 partial Δ variant is referred to in this study as 9pΔ. We also detected two variants in the C terminal amino acid sequences [NLAYW-COOH (Type I) and NLAYWSTYLFRDEEEEK-COOH (Type II)] in the larval brain (Fig. 1B). No RNA editing resulting in amino acid mutations in BmGluCls was observed from the larval brain cDNAs.

A comparison of sequence identities as well as the use of a phylogenetic tree (Supplemental Fig. 1) shows that BmGluCl is most closely related to the GluCl of another lepidopteran insect, the diamond-back moth *Plutella xylostella*, sharing 90% identity. With GluCls of coleopteran, dipteran and hymenopteran insects, BmGluCl shows 77–83% identity. Compared to arachnids, BmGluCl shares considerably lower

Molecular Pharmacology Fast Forward. Published on September 26, 2014 as DOI: 10.1124/mol.114.095869
This article has not been copyedited and formatted. The final version may differ from this version.

identity, showing 49% identity with the red spider mite *Tetranychus urticae*, and lower identity still when compared to nematode GluCls (39% and 36% with GLC-1 and GLC-2, respectively).

From the 50 Type II clones analysed, we found exon 3b (48%) to be the most abundant, followed by exon 3c (40%), exon 3a (10%); and exon 3Δ (2%) (Fig. 1C). The deletion of exon 3 resulting from an in-frame stop codon led to the generation of an incomplete, non-functional BmGluCl. Leaving aside exon 3Δ, the detection frequency for variants containing the exon 9 and 9 pΔ were 90% and 8%, respectively (Fig. 1D).

BmGluCl gene expression

We quantified the *BmGluCl* gene expression in the larval nervous system. The order of abundance of BmGluCl splice variants was exon 3b, exon 3c > exon 3a > exon 3Δ (Fig. 1E). Also, variants containing exon 9 complete were expressed at a much higher level than those containing the truncated version (Fig. 1F). The *GluCl* gene expression level in the third thoracic ganglion of the *Bombyx* larvae resembled those for the brain, with exons 3b and 3c being predominant (Fig. 1G). Also, the exon 9 complete variant was more abundant than the truncated counterpart (Fig. 1H).

Functional expression of BmGluCls in *Xenopus laevis* oocytes

The cRNA for each GluCl variant was injected into *X. laevis* oocytes to determine the concentration-response relationships for L-glutamate and IVM. Although BmGluCls carrying type I C-terminal sequence were not functionally expressed, those carrying type II C-terminal sequence combined with either exon 3a, exon 3b, exon 3b/exon 9pΔ (Accession number: KC342247), exon 3c or exon 3c/exon 9pΔ (Accession number: KC342248) formed robust

Molecular Pharmacology Fast Forward. Published on September 26, 2014 as DOI: 10.1124/mol.114.095869
This article has not been copyedited and formatted. The final version may differ from this version.

functional GluCls that responded to bath-applied 1 mM L-glutamate (Fig. 2A). However, the exon 3Δ variant was not functional because the transcript has an in-frame stop codon in the exon-3 coded sequence.

No significant difference was observed between variants in terms of pEC_{50} ($-logEC_{50}$) (Fig. 2B, C, Table 1) when current amplitude data were plotted against the concentration of L-glutamate. In contrast, approximately 3.6-fold differences were noted in the amplitude of the peak response to L-glutamate. The amplitude of the peak response was highest for exon 3c variant, followed respectively by exon 3b and exon 3a variants (Fig. 2B, D, Table 1). The differences between exon 3a vs 3c, between exon 3a vs exon 3c/exon 9pΔ, between exon 3b vs exon 3c/exon 9pΔ and between exon 3b/exon 9pΔ vs exon 3c/exon 9pΔ were all significant ($p < 0.05$, by Tukey's test (one-way ANOVA)). However, the effect of the exon 9 truncation on the L-glutamate response was not significant.

We also tested IVM on the BmGluCl variants expressed in *Xenopus* oocytes. IVM-induced inward currents (Fig. 2E) increased and decayed more slowly than the L-glutamate-induced currents (Fig. 2A). As found for L-glutamate, IVM activated each variant with similar EC_{50} (Fig. 2F, G), but with the maximum current amplitude changing with the variation in sequences at exon 3 (Fig. 2H). The exon 3c and exon 3c/exon 9pΔ variants showed significantly larger responses to IVM than the exon 3a variant ($p < 0.05$, by Tukey's test (one-way ANOVA)) (Fig. 2F, H, Table 1).

[^{3}H]IVM binding to oocyte and HEK293 cell membranes expressing BmGluCl variants

We measured specific binding of 1 nM [^{3}H]IVM to *Xenopus* oocyte membranes expressing splice variants of BmGluCls at a saturating concentration of IVM (1 μM) (Fig. 2I). [^{3}H]IVM bound at the lowest level of 35 ± 11 fmol/mg protein to oocyte membranes expressing the exon

Molecular Pharmacology Fast Forward. Published on September 26, 2014 as DOI: 10.1124/mol.114.095869
This article has not been copyedited and formatted. The final version may differ from this version.

3a variant, whereas it bound at the highest level (197 ± 76 fmol/mg protein) to membranes expressing the exon 3c variant, with binding to membranes of the exon 3b variant at an intermediate level (96 ± 13 fmol/mg protein) (Fig. 2I). A significant difference of the specific [^{3}H]IVM binding was observed when the exon 3a and exon 3c variants were compared ($p < 0.05$, by Tukey's test (one-way ANOVA)).

We further conducted [^{3}H]IVM binding assay using HEK293 cells expressing the exon 3a, 3b, 3c and exon 3c/exon 9pΔ variants (Fig. 2J). The cDNAs of variants were expressed at a similar level in the cell as evaluated by semi-quantitative RT-PCR (Fig. 2J, left). No significant specific [^{3}H]IVM binding was observed for cells expressing the exon 3a variant, whereas significant binding was detected from cells expressing other variants (Fig. 2J, middle). [^{3}H]IVM bound with a B_{max} order of exon 3c (656.2 ± 85.7 fmol/mg protein) > exon 3c/exon 9pΔ (316.9 ± 31.5 fmol/mg protein) > exon 3b (243.6 ± 31.7 fmol/mg protein) (Fig. 2J right), whereas there was no significant difference in K_d [exon 3b, 222 ± 99 pM (mean ± SEM, n = 3); exon 3c, 268 ± 113 pM (n = 3); exon 3c/exon 9pΔ, 217 ± 75 pM (n = 3)].

Amino acid residues determining the response amplitude of BmGluCl variants to L-glutamate and IVM

To identify structural features of the exon 3c coding region underpinning enhanced responses to L-glutamate and IVM, we first divided the region into two parts, blocks I and II, and exchanged each block between exon 3a and 3c GluCl isomers (Fig. 1B). Exchanging block I had no significant impact on the response amplitude to L-glutamate and IVM (Fig. 3A, B), except for the IVM response of the exon 3c chimera when the block was replaced with that of the exon 3a variant (Fig. 3 B). In contrast, replacing block II of exon 3a with that of exon 3c resulted in enhanced amplitude to the responses to L-glutamate and IVM (Fig. 3C), whereas an inverse

Molecular Pharmacology Fast Forward. Published on September 26, 2014 as DOI: 10.1124/mol.114.095869
This article has not been copyedited and formatted. The final version may differ from this version.

exchange in exon 3c resulted in reduced responses (Fig. 3D), indicating that block II played a more important role than block I in determining the response amplitude.

In Block II, Thr77, Thr78, Ser80 and Ile82 of exon 3a isomer differs from corresponding amino acids (Ser78, Lys79, Asp81 and Tyr83) of exon 3c isomer (Fig. 1). Hence, these four amino acids were exchanged either singly, or in combinations, between exon 3a and 3c splice variants and resultant mutants were expressed in *Xenopus* oocytes to identify which amino acid(s) has a critical role in determining response amplitude to L-glutamate. Replacing one or two of these four amino acids in exon 3a variant did not yield significantly higher responses than those seen in wild type (Fig. 3E). However, when any three amino acids of the four were combined to replace with the corresponding exon 3c amino acids (T77S;T78K;S80D, T77S;T78K;I82Y, T77S;S80D; I82Y, T78K;S80D; I82Y), the amplitude of the response became significantly greater than that of the wild type response (Fig. 3E, n = 4, $p < 0.05$, one-way ANOVA, Tukey's test). Among the triple mutations, the T78K;S80D;I82Y triple mutation had a greatest effect on the L-glutamate response (Fig. 3E)

We also examined the effects of single amino acid mutations in the exon 3c variant, changing to the corresponding amino acids found in exon 3a. Of the four single amino acid mutations, only S78T and Y83I mutations significantly reduced the current amplitude of the response to L-glutamate as compared with the control (Fig. 3F, n = 4, $p < 0.05$, one-way ANOVA, Tukey's test).

Similar results were obtained when the impacts of single, double and triple mutations were examined on the response to IVM (Fig. 3G). When three of Thr77, Thr78, Ser80 and Ile82 in block II of exon 3a variant were substituted by corresponding amino acids in exon 3c variant, the response amplitude to IVM significantly increased as compared with the response of the wild type exon 3a variant. The impact of T78K;S80D;I82Y triple mutation on the IVM response

Molecular Pharmacology Fast Forward. Published on September 26, 2014 as DOI: 10.1124/mol.114.095869
This article has not been copyedited and formatted. The final version may differ from this version.

was greatest among the four triple mutations (Fig. 3G). For the effects of mutations on IVM response of exon 3c variant, not only S78T and Y83I mutations, but also a K79T mutation, significantly reduced the response amplitude to IVM (Fig. 3H, n = 4, $p < 0.05$, one-way ANOVA, Tukey's test), yet the impact of K79T mutation was smaller than the impacts of S78T and Y83I mutations .

Modeling of GluCl variants

To elucidate the mechanism for the receptor-density determining effects of the exon 3-coding sequence, the BmGluCl exon 3a and 3c variants complexed with L-glutamate and IVM were modeled using the crystal structure of *C. elegans* GluCl α subunit (Fig. 4A, B) (Hibbs and Gouaux, 2011). Block I is located close to or at the L-glutamate-binding domain (Fig. 4C, E), whereas block II is present at the interface of neighboring two subunits (Fig. 4D, F). In block II of the exon 3a splice variant model, Thr77 and Thr78 do not appear to have a particular role, whereas Lys83 forms a salt bridge with Glu85 (Fig. 4E). On the other hand, in block II of the exon 3c splice variant, Lys79 of one subunit forms a salt bridge with Glu86 of another subunit where Asp81 forms a salt bridge with Lys84 (Fig. 4F). Additionally, Tyr83 contacts TM2–TM3 linker (Fig. 4F).

Molecular Pharmacology Fast Forward. Published on September 26, 2014 as DOI: 10.1124/mol.114.095869
This article has not been copyedited and formatted. The final version may differ from this version.

Discussion

Lepidopteran larvae are among the world's most important agricultural pests. Lepidopteran adults can also be beneficial pollinators and in the case of *Bombyx mori* larvae are important for commercial silk production. Thus, Lepidoptera present complex challenges for sustaining the world's harvest and for other important industries. The cys-loop LGICs are targets for several of the current generation of crop protection chemicals (Raymond-Delpech et al., 2005), but to date there are very few studies of cloned and functionally expressed lepidopteran cys-loop LGICs. In this study we describe for the first time robust functional expression of *B. mori* GluCls. We also provide the first study of the effects of splicing-induced diversity on the pharmacology of the GluCls expressed in the brain and third thoracic ganglion of the last instar larvae. Functional diversity is generated by the incorporation of one of three alternatives for exon 3 (Fig. 1A). The equivalent exon is also spliced in other insects although the number of possible alternative exons can vary between species. For instance, there are three possible alternatives for the GluCls in *Tribolium castaneum* (Jones and Sattelle, 2007), *Apis mellifera* (Demares et al., 2013) and *Musca domestica* (Kita et al., 2013), whereas only two are found in *Drosophila melanogaster* (Semenov and Pak, 1999) and *Nasonia vitripennis* (Jones et al., 2010). The variant we observed here where exon 3 is omitted (Fig. 1B) has so far only been seen in the GluCl of *B. mori*. However, the exclusion of exons has been observed in other insect cys-loop ligand-gated ion channels such as the α6 nicotinic acetylcholine receptor subunit (Grauso et al., 2002).

In *Drosophila* GluCl, diversity is also increased by the addition of a small number of residues at the C-terminus (Semenov and Pak, 1999), which we found also to be the case for BmGluCl (Fig. 1B). The complete exon 9 encoded sequence in *Bombyx* may be considered as an insertion from the partially Δ sequence. However, the frequency of the complete exon 9

Molecular Pharmacology Fast Forward. Published on September 26, 2014 as DOI: 10.1124/mol.114.095869
This article has not been copyedited and formatted. The final version may differ from this version.

sequence was higher than that of the truncated one (Fig. 1). Hence we depict the longer exon 9-encoded sequence as the norm (Fig. 1B).

In *Drosophila* GluCl, several residues undergo RNA editing (Semenov and Pak, 1999). We found no amino-acid changing RNA editing in the BmGluCl message from the larval brain. However, we cannot rule out that editing of BmGluCl may occur in adults, as much lower editing was observed in the embryo and larval stages than in adult stages in the case of the *Drosophila* GABA receptor, RDL (Jones et al., 2009) and in general RNA editing is more pronounced in adult insect nervous tissue (Keegan et al., 2005).

We detected two C-terminal sequences Types I and II (Fig. 1B). The variant with Type I C terminal was not functional on its own. Type I variant, as well as the peptide resulting from the deletion at exon 3, may prevent functional expression of other splice variants, resulting in a dominant negative effect. In such an event, inhibitory control in the nervous system would be reduced, leading to enhanced excitability which may accelerate hatching, molting and eclosion.

For the *Drosophila* RDL GABA receptor, alternative splicing as well as RNA editing profoundly affected the EC_{50} for GABA (Jones et al., 2009). In contrast, the splicing-induced variations in BmGluCl scarcely influence the EC_{50} for L-glutamate and IVM. Alternative splicing of the *Musca domestica* GluCl was also found not to affect L-glutamate sensitivity (Kita et al., 2013). However, we show that such diversity at exon 3 resulted in dramatic changes in the peak amplitude of the responses to L-glutamate (Fig. 2D) and IVM (Fig. 2H). The rank order of exon 3c > exon 3b > exon 3a for [^{3}H]IVM binding to BmGluCls expressed in oocytes (Fig. 2I) and HEK293 cells (Fig. 2J) resembles the rank order of the response amplitude to L-glutamate and IVM (Figs. 2D, H), suggesting that the changes in the response amplitude, at least in part, result from those in the cell-surface receptor numbers. However, such phenomena may be limited to the vertebrate expression vehicles deployed in this study, *Xenopus* oocytes

and HEK293 cells. Thus, studies using insect cell lines are needed in the future prior to any broader conclusion that the exon-3-coded amino acids always regulate the functional expression of GluCls.

Amino acids have also been identified that influence the membrane traffic of LGICs other than BmGluCls. For example, the amino acid (Arg607) in the RNA editing site of the AMPA-type glutamate receptor subunit GluA2 has been recognized as a determinant of membrane trafficking and thus, cell surface density (Greger et al., 2002). Notably, RNA editing at Arg607 controls the AMPA receptor exit from the endoplasmic reticulum (ER). Also, RNA-editing in the ligand binding domain and subunit interface of AMPA receptors has been shown to alter surface expression through the quality check at ER (Penn and Greger, 2009). In the case of vertebrate GABA receptor subunit α3, the editing-induced Ile to Met switch in TM3 has been shown to reduce its expression in HEK293 cells (Daniel et al., 2011). We have identified 4 amino acids as key determinants of the cell-surface receptor numbers of BmGluCls (Fig. 3). In the case of the GluA2 receptor, stronger interface contacts result in prolonged ER retention, thereby enhancing receptor biogenesis. Of the 4 key amino acids in BmGluCls, 3 are involved in inter-subunit contacts at the subunit interface (Fig. 4). These amino acids may determine the ER retention time and thus, membrane trafficking. However, if the difference of the response amplitude of BmGluCl variants was solely due to trafficking, then radioligand binding to the splice variants would be similar, but this was not the case. Therefore, the difference in ligand binding may be due to differences in assembly of the subunits into a functional pentamer or translation efficiency of the cRNAs.

In the computationally-generated model, only one salt bridge is formed between Lys83 and Glu85 within each subunit of the exon 3a variant (Fig. 4E). In addition to one within-subunit salt bridge formed between Asp81 and Lys84, an inter-subunit salt bridge between Lys79 and

Molecular Pharmacology Fast Forward. Published on September 26, 2014 as DOI: 10.1124/mol.114.095869
This article has not been copyedited and formatted. The final version may differ from this version.

Glu86 in a separate subunit is formed in the exon 3c variant (Fig. 4F), strengthening subunit assembly. However, the K79T mutation in the exon 3c variant had no significant effect on the response amplitude to L-glutamate (Fig. 3F) and only a small impact on the response amplitude to IVM (Fig. 3H). At first glance, this appears to contradict the salt bridge-assisted assembly mechanism, yet the observation can be accounted as follows. Ser78 assists in Lys79 access to Glu86, promoting the assembly and, in the K79T mutant, Ser78 forms a hydrogen bond with Glu86, counteracting the loss of Lys79–Asp81 salt bridge.

In this way, the diversified response in current amplitude of BmGluCl variants can be explained, in part, by the changes of receptor density. Nevertheless, the factors influencing the current amplitude are not limited to just to this process. The Tyr83 in exon 3c interacts with the TM2–TM3 linker (see Fig. 4F), whereas Ile82 in exon 3a does not contact the linker (Fig. 4E). Since the TM2–TM3 linker is located close to the transmembrane allosteric site (Hibbs and Gouaux, 2011), such a Tyr83 contact may promote gating of the ion channel, resulting in higher current amplitude of the IVM response. Alternatively, the stabilized open conformation may accelerate exit from the ER, thereby enhancing the number of functional BmGluCls as in the case of ionotropic L-glutamate-gated cation channels (Coleman et al., 2009; Fleck, 2006; Gill et al., 2009; Penn et al., 2008).

In addition to the interactions with the linker, we cannot also rule out a possible contribution of block I to the observed amplitude variations. Thr77 in exon 3a and Ser78 in exon 3c are located in the vicinity of block I where L-glutamate binds (Fig. 4). Thus, these connecter amino acids may indirectly affect the response amplitude. Indeed, the exon 3a chimera where only block II region was replaced with the corresponding exon 3c region (Fig. 3C) showed smaller amplitudes of the L-glutamate and IVM responses than those of the wild type exon 3c variant (Fig. 3B), reflecting some block I contributions to the determination of the

Molecular Pharmacology Fast Forward. Published on September 26, 2014 as DOI: 10.1124/mol.114.095869
This article has not been copyedited and formatted. The final version may differ from this version.

response amiplitude. Also, the effects of the mutations of amino acids in block II of the two variants were not complete mirror images (Fig. 4E–H), further supporting this. Nonetheless, we show that mutations of the four amino acids in block II can affect the GluCl response amplitude to the orthosteric ligand L-glutamate and the allosteric ligand IVM (Fig. 3E–H).

Thus, from our own and other studies, exon 3 splicing is now known to affect both ligand-gated anion channel cell surface expression levels and affinity for ligands, thereby influencing apparent EC_{50} and efficacy, respectively. For the first time we have shown that 4 residues (Thr77, Thr78, Ser80 and Ile82 in the exon 3a variant; Ser78, Lys79, Asp81 and Tyr83 in the exon 3c variant) can influence cell surface receptor density. The splice variants of BmGluCls expressed in the brain and the third thoracic ganglion show diverse amplitudes in response to L-glutamate and IVM depending on the level of cell surface expression. It is important to examine whether such GluCl regulation is general in insects and can be extended to other cys-loop LGICs. It will also be of interest to elucidate the role of non-sense variants, which may offer a possible a means of down-regulating inhibitory neurotransmission, as is the case for the mouse α7 nAChR subunit, where a truncated variant acts as a dominant negative when co-transfected with full-length α7 in HEK 293 cells (Saragoza et al., 2003).

The BmGluCl studies enhance our current understanding of the diverse functional impact of ligand-gated anion channel exon 3 splicing on the response to orthosteric and allosteric ligands.

Molecular Pharmacology Fast Forward. Published on September 26, 2014 as DOI: 10.1124/mol.114.095869
This article has not been copyedited and formatted. The final version may differ from this version.

Acknowledgements

We acknowledge Dr Hiroaki Noda and Dr. Yukiko Matsumoto of National Institute of Agricultural Sciences for assistance in cloning and sequencing the cDNAs. We thank Dr. Keiji Tanaka of Kinki University for assistance in the binding assay and Professor Yoshihisa Ozoe, Dr. Tomo Kita, Mr. Takahiro Irie and Toshinori Fuse of Shimane University for advice on the binding assay. We also thank Dr. Hirokazu Ueda of National Institute for Agro-Environmental Sciences for assistance in the quantitative PCR.

Authorship contribution

Participated in research design: Matsuda, Sattelle

Conducted experiments: Furutani, Ihara, Nishino, Akamatsu, Jones

Performed data analysis: Furutani, Ihara, Jones, Sattelle, Matsuda

Wrote or contributed to the writing of the manuscript: Furutani, Ihara, Nishino, Akamatsu, Jones, Sattelle, Matsuda

References

Buckingham SD, Biggin PC, Sattelle BM, Brown LA and Sattelle DB (2005) Insect GABA receptors: splicing, editing, and targeting by antiparasitics and insecticides. *Mol Pharmacol* **68**:942-951.

Coleman SK, Moykkynen T, Jouppila A, Koskelainen S, Rivera C, Korpi ER and Keinanen K (2009) Agonist occupancy is essential for forward trafficking of AMPA receptors. *J Neurosci* **29**:303-312.

Cull-Candy SG (1976) Two types of extrajunctional L-glutamate receptors in locust muscle fibres. *J Physiol* **255**:449-464.

Cully DF, Paress PS, Liu KK, Schaeffer JM and Arena JP (1996) Identification of a *Drosophila melanogaster* glutamate-gated chloride channel sensitive to the antiparasitic agent avermectin. *J Biol Chem* **271**:20187-20191.

Cully DF, Vassilatis DK, Liu KK, Paress PS, Van der Ploeg LH, Schaeffer JM and Arena JP (1994) Cloning of an avermectin-sensitive glutamate-gated chloride channel from *Caenorhabditis elegans*. *Nature* **371**:707-711.

Daniel C, Wahlstedt H, Ohlson J, Bjork P and Ohman M (2011) Adenosine-to-inosine RNA editing affects trafficking of the γ-aminobutyric acid type A ($GABA_{(A)}$) receptor. *J Biol Chem* **286**:2031-2040.

Demares F, Raymond V and Armengaud C (2013) Expression and localization of glutamate-gated chloride channel variants in honeybee brain (*Apis mellifera*). *Insect Biochem Mol Biol* **43**:115-124.

ffrench-Constant RH and Rocheleau TA (1993) *Drosophila* γ-aminobutyric acid receptor gene *Rdl* shows extensive alternative splicing. *J Neurochem* **60**:2323-2326.

Fleck MW (2006) Glutamate receptors and endoplasmic reticulum quality control: looking beneath the surface. *Neuroscientist* **12**:232-244.

Gengs C, Leung HT, Skingsley DR, Iovchev MI, Yin Z, Semenov EP, Burg MG, Hardie RC and Pak WL (2002) The target of *Drosophila* photoreceptor synaptic transmission is a histamine-gated chloride channel encoded by *ort* (*hclA*). *J Biol Chem* **277**:42113-42120.

Gill MB, Vivithanaporn P and Swanson GT (2009) Glutamate binding and conformational flexibility of ligand-binding domains are critical early determinants of efficient kainate receptor biogenesis. *J Biol Chem* **284**:14503-14512.

Gisselmann G, Pusch H, Hovemann BT and Hatt H (2002) Two cDNAs coding for histamine-gated ion channels in *D. melanogaster*. *Nat Neurosci* **5**:11-12.

Grauso M, Reenan RA, Culetto E and Sattelle DB (2002) Novel putative nicotinic acetylcholine receptor subunit genes, Dα5, Dα6 and Dα7, in *Drosophila melanogaster* identify a new and highly conserved target of adenosine deaminase acting on RNA-mediated A-to-I pre-mRNA editing. *Genetics* **160**:1519-1533.

Greger IH, Khatri L and Ziff EB (2002) RNA editing at Arg607 controls AMPA receptor exit from the endoplasmic reticulum. *Neuron* **34**:759-772.

Halgren TA (1999a) MMFF VI. MMFF94s option for energy minimization studies. *J Comput Chem* **20**:720-729.

Halgren TA (1999b) MMFF VII. Characterization of MMFF94, MMFF94s, and other widely available force fields for conformational energies and for intermolecular-interaction energies and geometries. *J Comput Chem* **20**:730-748.

Hardie RC (1989) A histamine-activated chloride channel involved in neurotransmission at a photoreceptor synapse. *Nature* **339**:704-706.

Hibbs RE and Gouaux E (2011) Principles of activation and permeation in an anion-selective Cys-loop receptor. *Nature* **474**:54-60.

Jones AK, Bera AN, Lees K and Sattelle DB (2010) The cys-loop ligand-gated ion channel gene superfamily of the parasitoid wasp, *Nasonia vitripennis. Heredity* **104**:247-259.

Jones AK, Buckingham SD, Papadaki M, Yokota M, Sattelle BM, Matsuda K and Sattelle DB (2009) Splice-variant- and stage-specific RNA editing of the Drosophila GABA receptor modulates agonist potency. *J Neurosci* **29**:4287-4292.

Jones AK and Sattelle DB (2006) The cys-loop ligand-gated ion channel superfamily of the honeybee, *Apis mellifera*. *Invert Neurosci* **6**:123-132.

Jones AK and Sattelle DB (2007) The cys-loop ligand-gated ion channel gene superfamily of the red flour beetle, *Tribolium castaneum. BMC Genomics* **8**:327.

Jones AK and Sattelle DB (2008) The cys-loop ligand-gated ion channel gene superfamily of the nematode, *Caenorhabditis elegans. Invert Neurosci* **8**:41-47.

Keegan LP, Brindle J, Gallo A, Leroy A, Reenan RA and O'Connell MA (2005) Tuning of RNA editing by ADAR is required in *Drosophila*. *EMBO J* **24**:2183-2193.

Kita T, Ozoe F and Ozoe Y (2013) Expression pattern and function of alternative splice variants of glutamate-gated chloride channel in the housefly *Musca domestica*. *Insect Biochem Mol Biol* **45C**:1-10.

Lees K, Jones AK, Matsuda K, Akamatsu M, Sattelle DB, Woods DJ and Bowman AS (2014) Functional characterisation of a nicotinic acetylcholine receptor alpha subunit from the brown dog tick, *Rhipicephalus sanguineus.* Int J Parasitol 44: 75-81.

Mita K, Kasahara M, Sasaki S, Nagayasu Y, Yamada T, Kanamori H, Namiki N, Kitagawa M, Yamashita H, Yasukochi Y, Kadono-Okuda K, Yamamoto K, Ajimura M, Ravikumar G, Shimomura M, Nagamura Y, Shin IT, Abe H, Shimada T, Morishita S and Sasaki T (2004) The genome sequence of silkworm, *Bombyx mori*. *DNA Res* **11**:27-35.

Pantazis A, Segaran A, Liu CH, Nikolaev A, Rister J, Thum AS, Roeder T, Semenov E, Juusola M and Hardie RC (2008) Distinct roles for two histamine receptors (*hclA* and *hclB*) at the *Drosophila* photoreceptor synapse. *J Neurosci* **28**:7250-7259.

Penn AC and Greger IH (2009) Sculpting AMPA receptor formation and function by alternative RNA processing. *RNA Biol* **6**:517-521.

Penn AC, Williams SR and Greger IH (2008) Gating motions underlie AMPA receptor secretion from the endoplasmic reticulum. *EMBO J* **27**:3056-3068.

Putrenko I, Zakikhani M and Dent JA (2005) A family of acetylcholine-gated chloride channel subunits in *Caenorhabditis elegans*. *J Biol Chem* **280**:6392-6398.

Raymond-Delpech V, Matsuda K, Sattelle BM, Rauh JJ and Sattelle DB (2005) Ion channels: molecular targets of neuroactive insecticides. *Invert Neurosci* **5**:119-133.

Raymond V and Sattelle DB (2002) Novel animal-health drug targets from ligand-gated chloride channels. *Nat Rev Drug Discov* **1**:427-436.

Ringstad N, Abe N and Horvitz HR (2009) Ligand-gated chloride channels are receptors for biogenic amines in *C. elegans*. *Science* **325**:96-100.

Saragoza PA, Modir JG, Goel N, French KL, Li L, Nowak MW and Stitzel JA (2003) Identification of an alternatively processed nicotinic receptor α7 subunit RNA in mouse brain. *Brain Res Mol Brain Res* **117**:15-26.

Semenov EP and Pak WL (1999) Diversification of *Drosophila* chloride channel gene by multiple posttranscriptional mRNA modifications. *J Neurochem* **72**:66-72.

Wafford KA and Sattelle DB (1986) Effects of amino acid neurotransmitter candidates on an identified insect motoneurone. *Neurosci Lett* **63**:135-140.

Wolstenholme AJ (1997) Glutamate-gated Cl- channels in *Caenorhabditis elegans* and parasitic nematodes. *Biochem Soc Trans* **25**:830-834.

Wolstenholme AJ (2012) Glutamate-gated Chloride Channels. *J Biol Chem*.

Wolstenholme AJ, Bowman AS and Sattelle DB (2007) Frontiers in parasite neurobiology: parasite genomics, neural signalling and new targets for control. *Invert Neurosci* **7**:179-181.

Wolstenholme AJ and Rogers AT (2005) Glutamate-gated chloride channels and the mode of action of the avermectin/milbemycin anthelmintics. *Parasitology* **131 Suppl**:S85-95.

Xia Q, Zhou Z, Lu C, Cheng D, Dai F, Li B, Zhao P, Zha X, Cheng T, Chai C, Pan G, Xu J, Liu C, Lin Y, Qian J, Hou Y, Wu Z, Li G, Pan M, Li C, Shen Y, Lan X, Yuan L, Li T, Xu H, Yang G, Wan Y, Zhu Y, Yu M, Shen W, Wu D, Xiang Z, Yu J, Wang J, Li R, Shi J, Li H, Su J, Wang X, Zhang Z, Wu Q, Li J, Zhang Q, Wei N, Sun H, Dong L, Liu D, Zhao S, Zhao X, Meng Q, Lan F, Huang X, Li Y, Fang L, Li D, Sun Y, Yang Z, Huang Y, Xi Y, Qi Q, He D, Huang H, Zhang X, Wang Z, Li W, Cao Y, Yu Y, Yu H, Ye J, Chen H, Zhou Y, Liu B, Ji H, Li S, Ni P, Zhang J, Zhang Y, Zheng H, Mao B, Wang W, Ye C, Wong GK and Yang H (2004) A draft sequence for the genome of the domesticated silkworm (*Bombyx mori*). *Science* **306**:1937-1940.

Zheng Y, Hirschberg B, Yuan J, Wang AP, Hunt DC, Ludmerer SW, Schmatz DM and Cully DF (2002) Identification of two novel *Drosophila melanogaster* histamine-gated chloride channel subunits expressed in the eye. *J Biol Chem* **277**:2000-2005.

Molecular Pharmacology Fast Forward. Published on September 26, 2014 as DOI: 10.1124/mol.114.095869
This article has not been copyedited and formatted. The final version may differ from this version.

Footnotes

This study was supported by a Grant-in-Aid for Scientific Research from the Japan Society for the Promotion of Science [Grants 21310147, 26292031]; the Integrated Research Project for Plants, Insects and Animals using Genome Technology from the Ministry of Agriculture, Forestry and Fisheries of Japan [Grant 1302]; and the Strategic Project to Support the Formation of Research Bases at Private Universities: Matching Fund Subsidy from the Ministry of Education, Culture, Sports, Science and Technology of Japan [Grant S1101035].

Molecular Pharmacology Fast Forward. Published on September 26, 2014 as DOI: 10.1124/mol.114.095869
This article has not been copyedited and formatted. The final version may differ from this version.

Figure legends

Figure 1. Genomic organization and diversified primary structure of *B. mori* glutamate-gated chloride channel (BmGluCls). (A) Intron-exon organization of the *BmGluCl* gene. (B) Primary structure of BmGluCl. Putative signal peptide is underlined. Transmembrane domains are indicated in blue, while variable amino acids at exon 3-coded sequence except for those of exon 3Δ variant are shown in red. Exon 3 encodes a part of the N-terminal ligand binding domain that is located upstream of the conserved cysteine residues colored green. Detection frequency of variant cDNAs generated by splicing at exon 3 (C) and exon 9 (D) from the cDNA library of *B. mori* larval brain. (E–H) Gene expression of BmGluCl variants determined by real-time PCR. Relative gene expression level of variants generated by splicing at exon 3 (E, G) and exon 9 (F, H) in the larval brain (E, F) and the third thoracic ganglion (G, H). Stage-dependent gene expression of BmGluCl variants generated at exon 3 (H) and exon 9 (I). The bar graphs are shown as the mean ± standard error (n = 3).

Molecular Pharmacology Fast Forward. Published on September 26, 2014 as DOI: 10.1124/mol.114.095869
This article has not been copyedited and formatted. The final version may differ from this version.

Figure 2. Inward current responses of BmGluCl splice variants to L-glutamate and ivermectin B_{1a} (IVM) and concentration-response relationships for these ligands. (A) Inward currents induced by 1 mM L-glutamate in *X. laevis* oocytes expressing BmGluCl splice variants. (B) Concentration response relationships for L-glutamate. (C) EC_{50}s for L-glutamate. (D) Maximum current amplitudes of variant responses to 1 mM L-glutamate. (E) Inward currents induced by 10 μM IVM in *X. laevis* oocytes expressing BmGluCl variants. (F) Concentration-response relationships for IVM. (G) EC_{50}s for L-glutamate. (H) Maximum current amplitudes (I_{max}) of the response to 10 μM IVM. The data shown in (B – D, F – H) are presented as the mean ± standard error of repeated experiments (n = 4). (I) Specific [^{3}H]IVM binding to membranes of *Xenopus* oocytes expressing BmGluCl variants. Twenty μg of protein was used for each assay. Data are represented as the mean ± standard error of repeated experiments (n = 3). (J) Specific [^{3}H]IVM binding to membranes of HEK293 cells expressing BmGluCl variants. (Left) RT-PCR of BmGluCl isoforms expressed in HEK293 cells as compared with the actin gene expression. (Middle) Specific binding of 1 nM [^{3}H]IVM to membranes (10 μg protein) of HEK293 cells expressing BmGluCl variants (n = 3). No detectable specific [^{3}H]IVM binding was observed to membranes of HEK293 cells transfected with the exon 3a variant cDNA. (Right) Saturation isotherms of specific [^{3}H]IVM binding to membranes (10 μg protein) of HEK293 cells expressing BmGluCl variants. Data are shown as the mean ± standard error (n = 3). A significant difference was observed in B_{max} between exon 3b and exon 3c variants ($p < 0.05$, one-way ANOVA), whereas no such a difference was observed in K_d for exon 3b, exon 3c and exon 3c/exon9pΔ variants. In (C, D, G, H – J), x, y or z indicate groups of data that are statistically different ($p < 0.05$, one-way ANOVA, Tukey's test).

Molecular Pharmacology Fast Forward. Published on September 26, 2014 as DOI: 10.1124/mol.114.095869
This article has not been copyedited and formatted. The final version may differ from this version.

Figure 3. The current amplitude of the responses to L-glutamate and ivermectin (IVM) of the wild type BmGluCl splice variants 3a and 3c and their chimeras and mutants. Each bar graph represented as mean ± standard error of the mean (n = 4 – 8). (A) Wild type exon 3a variant and its chimera containing exon 3c sequence in block I region. (B) Wild type exon 3c and its chimera containing exon 3a sequence in block I. (C) Wild type exon 3a and its chimera containing exon 3c sequence in block II region. (D) Wild type exon 3c and its chimera containing exon 3a sequence in block II region. (E) Responses to L-glutamate of the wild type exon 3a and its mutants where single–three amino acids were exchanged with corresponding amino acids in exon 3c in block II region. (F) Responses to L-glutamate of the wild type exon 3c and its mutants where a single amino acid was exchanged with the corresponding amino acid in exon 3a in block II region. (G) Responses to IVM of the wild type exon 3a and its mutants where single–three amino acids were exchanged with corresponding amino acids in exon 3c in block II region. (H) Responses to IVM of the wild type exon 3c and its mutants where a single amino acid was exchanged with the corresponding amino acid in exon 3a in block II region. In panels (E) – (H), the same wild type and chimera (block II 3a to 3a and block II 3c to 3a) data as those indicated in (C) and (D) were used to facilitate understanding the changes resulting from the amino acid swapping. In (A) – (D), the Student's *t*-tests were carried out (*, $p < 0.05$; **, $p < 0.01$). In (E) – (H), one-way ANOVA (Tukey's tests) were carried out. Different letters (a – e) were used to indicate groups showing significant differences ($p < 0.05$).

Molecular Pharmacology Fast Forward. Published on September 26, 2014 as DOI: 10.1124/mol.114.095869
This article has not been copyedited and formatted. The final version may differ from this version.

Figure 4. Molecular modeling of exon 3a and exon 3c variants of BmGluCls. Each model was constructed using PDFAMS Pro/Ligand&Complex software. L-Glutamate, ivermectin (IVM) and exon 3 coding amino acids are represented by space filling models. The main chain of the principal subunit containing loops A – C is colored yellow, whereas the complementary subunit containing loops D – F is colored blue. Models of the 3a splice variant in complex with L-glutamate and IVM are shown in (A), (C) and (E), whereas those of 3c are shown in (B), (D) and (F). In both ligands, carbon, hydrogen, oxygen and nitrogen atoms are colored white, cyan, red and blue, respectively. Between panels (A) and (B) and lower panels, amino acid sequences encoded by exon 3c are indicated. (C) – (F) Expanded views from inside the channel. In the exon 3 coding region, block I was colored orange, whereas block II was colored purple except for amino acids playing important roles in determining the GluCl response amplitude as follows. 3a amino acid/3c amino acid: Thr77/Ser78 (violet), Thr78/Lys79 (green), Ser80/Asp81 (green blue), Ile82/Tyr83 (red), Lys83/Lys84 (light green) and Glu85/Glu86 (pink). Salt bridges are indicated by arrows. The PDB files of exon 3a and exon 3c variant models are available in the supplemental data.

Molecular Pharmacology Fast Forward. Published on September 26, 2014 as DOI: 10.1124/mol.114.095869
This article has not been copyedited and formatted. The final version may differ from this version.

Legends for PDB files included as supplemental data

BmGluCl3a.pdb: Homology model of BmGluCl exon 3a variant

BmGluCl3c.pdb: Homology model of BmGluCl exon 3c variant

Molecular Pharmacology Fast Forward. Published on September 26, 2014 as DOI: 10.1124/mol.114.095869
This article has not been copyedited and formatted. The final version may differ from this version.

Table 1. EC_{50} and maximum current amplitude (I_{max}) of L-glutamate- and IVM-induced responses of BmGluCls expressed in *Xenopus laevis* oocytes

Variants	L-Glutamate		IVM	
	pEC_{50} (M)	I_{max} (μA)	pEC_{50} (M)	I_{max} (μA)
Exon 3a	4.51 ± 0.26	2.55 ± 0.25	6.26± 0.42	1.07 ± 0.16
Exon 3b	4.35 ± 0.23	4.21 ± 0.35	6.41 ± 0.32	3.20 ± 0.44
Exon 3b/Exon 9 partially Δ	4.48 ± 0.14	4.28 ± 0.22	6.43± 0.21	2.32 ± 0.33
Exon 3c	4.71 ± 0.19	9.56 ± 0.73	5.67 ± 0.09	4.82 ± 0.41
Exon 3c/Exon 9 partially Δ	4.70 ± 0.13	11.40 ± 0.62	5.85 ± 0.13	5.24 ± 0.57

Data were obtained by non-linear regression analyses (See Materials and Methods) and are indicated as mean ± standard error of the mean of repeated experiments (L-Glutamate, n = 4; IVM, n = 4).

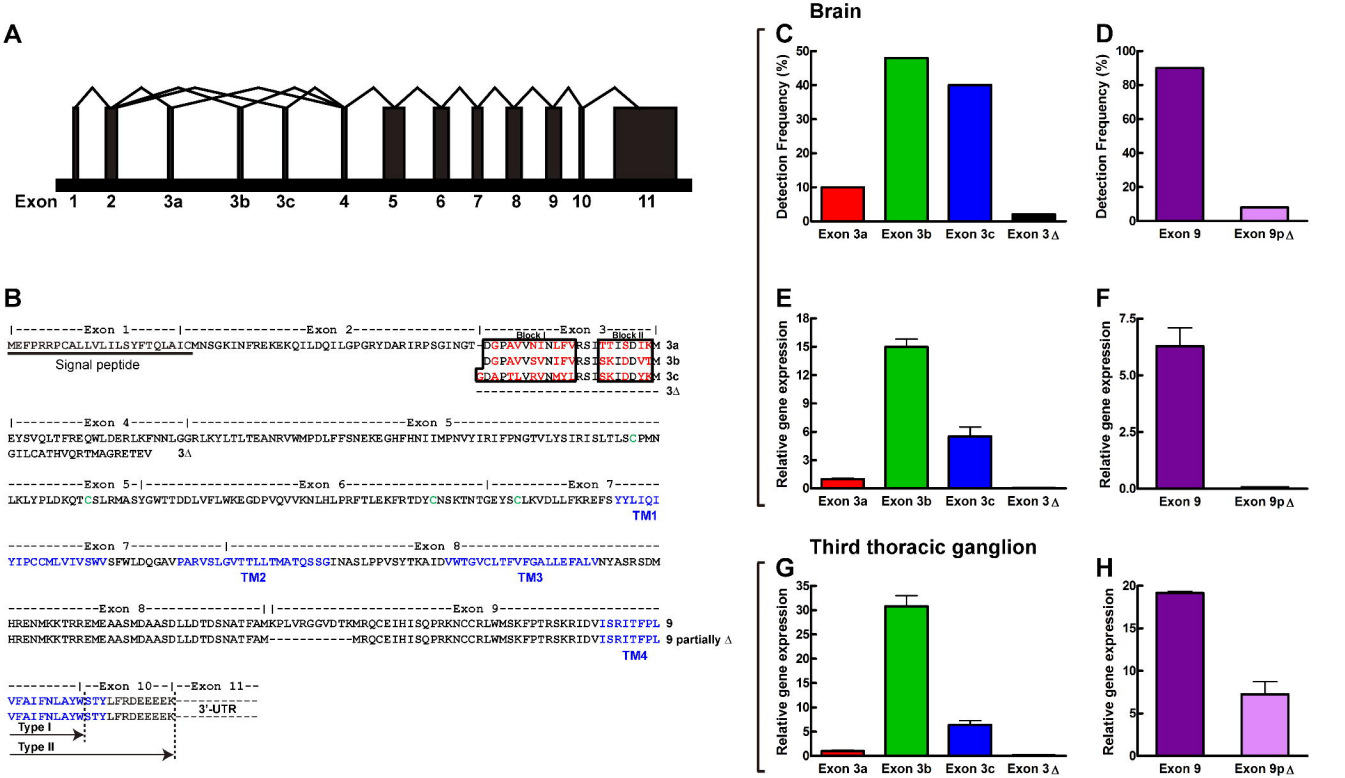
A
Exon 1 2 3a 3b 3c 4 5 6 7 8 9 10 11
B
Exon 1
Exon 2
Exon 3
Block I
Block II
MEFPRRPCALLVLILSYFTQLAICMNSGKINFREKEKQILDQILGPGRYDARIRPSGINGT-DGPAVVNINLFVRSIPTISDIRM 3a
Signal peptide
DGPAVVSVNIFVRSISKIDDVTM 3b
GDAPTLVEVNMYIRSISKIDDYKM 3c
3Δ
Exon 4
Exon 5
EYSVQLTFREQWLDERLKFNNLGGRLKYLTLTEANRVWMPDLFFSNEKEGHFHNIIMPNVYIRIFPNGTVLYSIRISLTLSCPMN
GILCATHVQRTMAGRETEV 3Δ
Exon 5
Exon 6
Exon 7
LKLYPLDKQTCSLRMASYGWTTDDLVFLWKEGDPVQVVKNLHLPRFTLEKFRTDYCNSKTNTGEYSCLKVDLLFKREFSYYLIQI
TM1
Exon 7
Exon 8
YIPCCMLVIVSWVSFWLDQGAVPARVSLGVTTLLTMATQSSGINASLPPVSYTKAIDVWTGVCLTFVFGALLEFALVNYASRSDM
TM2
TM3
Exon 8
Exon 9
HRENMKKTRREMEAASMDAASDLLDTDSNATFAMKPLVRGGVDTKMRQCEIHISQPRKNCCRLWMSKFPTRSKRIDVISRITFPL 9
HRENMKKTRREMEAASMDAASDLLDTDSNATFAM----------MRQCEIHISQPRKNCCRLWMSKFPTRSKRIDVISRITFPL 9 partially Δ
TM4
Exon 10
Exon 11
VFAIFNLAYWSTYLFRDEEEEK----------
VFAIFNLAYWSTYLFRDEEEEK----------
3'-UTR
Type I
Type II
Brain
C
Detection Frequency (%)
Exon 3a
Exon 3b
Exon 3c
Exon 3Δ
D
Detection Frequency (%)
Exon 9
Exon 9pΔ
E
Relative gene expression
Exon 3a
Exon 3b
Exon 3c
Exon 3Δ
F
Relative gene expression
Exon 9
Exon 9pΔ
Third thoracic ganglion
G
Relative gene expression
Exon 3a
Exon 3b
Exon 3c
Exon 3Δ
H
Relative gene expression
Exon 9
Exon 9pΔ

Figure 1

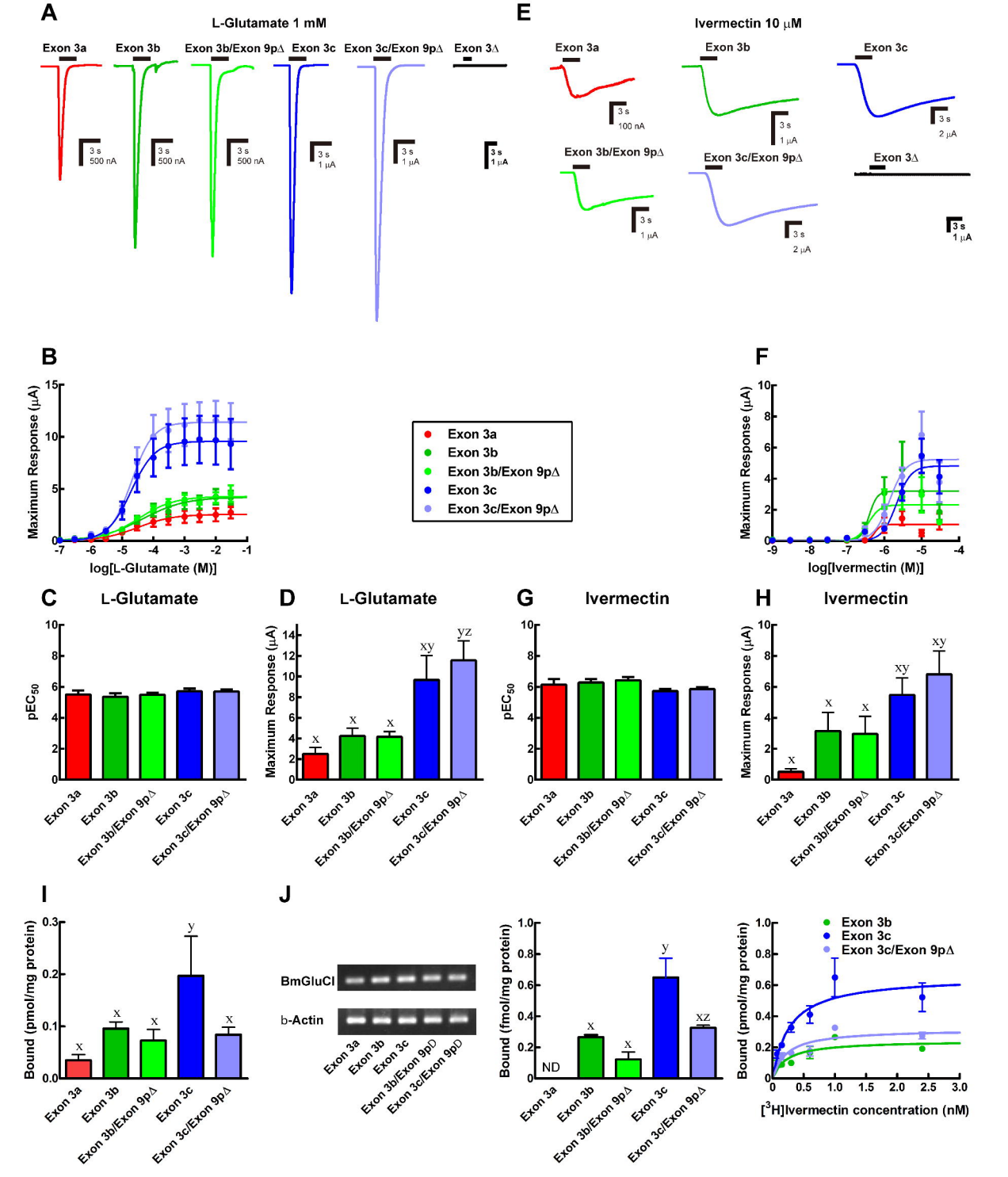
A
L-Glutamate 1 mM
Exon 3a
Exon 3b
Exon 3b/Exon 9pΔ
Exon 3c
Exon 3c/Exon 9pΔ
Exon 3Δ
E
Ivermectin 10 μM
B
Maximum Response (μA)
log[L-Glutamate (M)]
Exon 3a
Exon 3b
Exon 3b/Exon 9pΔ
Exon 3c
Exon 3c/Exon 9pΔ
F
Maximum Response (μA)
log[Ivermectin (M)]
C
L-Glutamate
pEC50
D
L-Glutamate
Maximum Response (μA)
G
Ivermectin
pEC50
H
Ivermectin
Maximum Response (μA)
I
Bound (pmol/mg protein)
J
BmGluCl
b-Actin
Bound (fmol/mg protein)
ND
Bound (pmol/mg protein)
[3H]Ivermectin concentration (nM)

Figure 2.

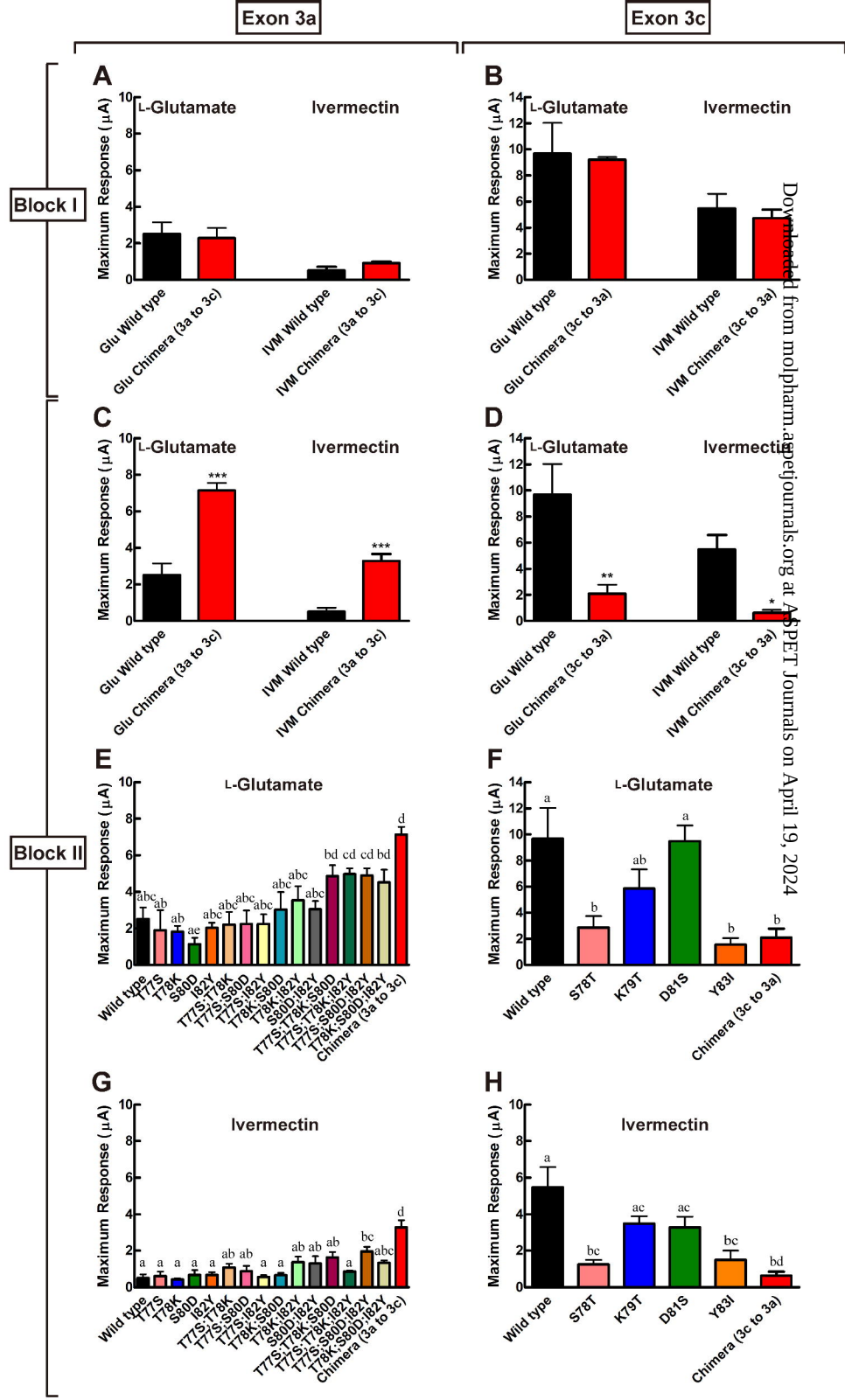

Figure 3.

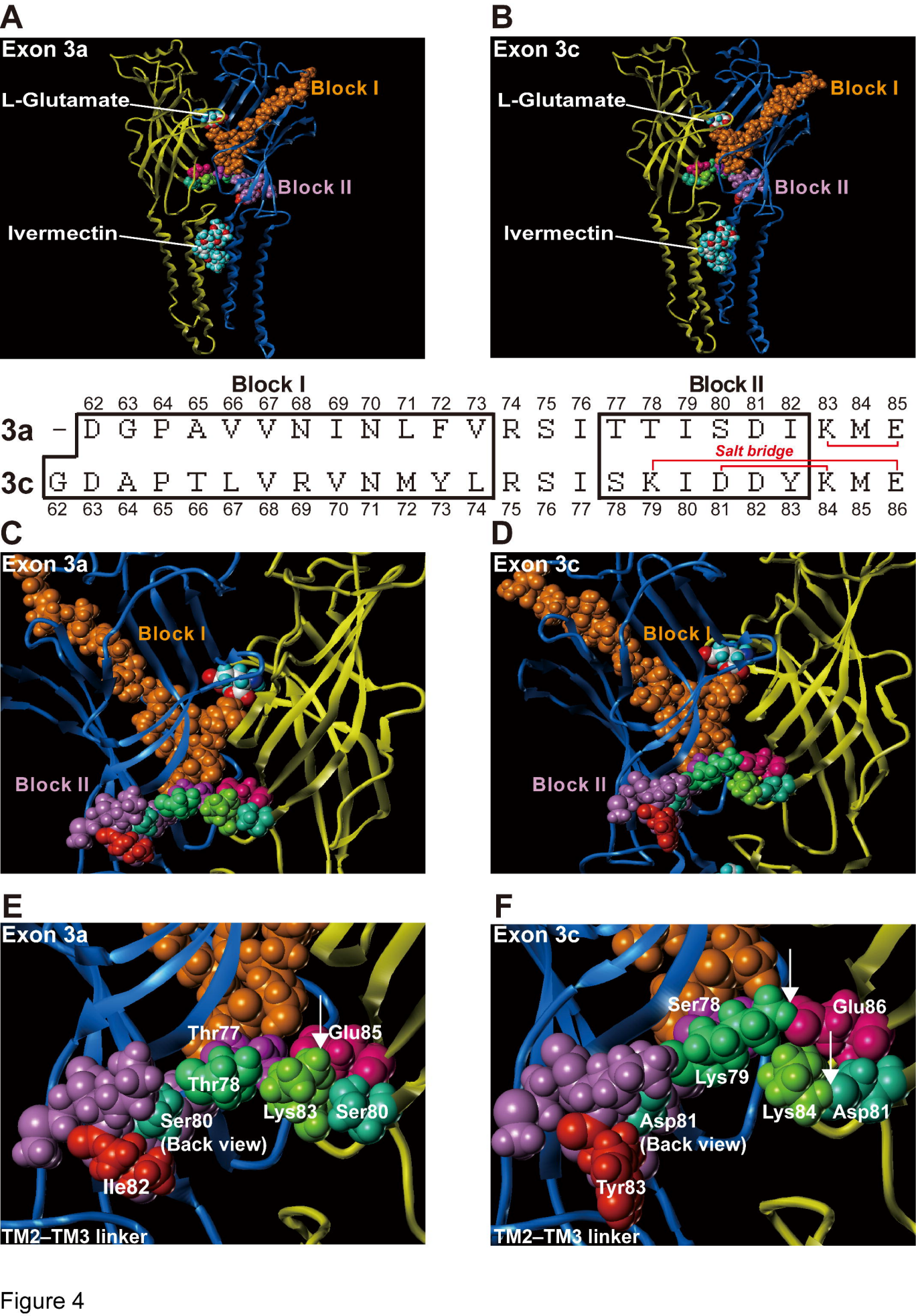
A
Exon 3a
L-Glutamate
Block I
Block II
Ivermectin
B
Exon 3c
L-Glutamate
Block I
Block II
Ivermectin
Block I
Block II
62 63 64 65 66 67 68 69 70 71 72 73 74 75 76 77 78 79 80 81 82 83 84 85
3a – D G P A V V N I N L F V R S I T T I S D I K M E
Salt bridge
3c G D A P T L V R V N M Y L R S I S K I D D Y K M E
62 63 64 65 66 67 68 69 70 71 72 73 74 75 76 77 78 79 80 81 82 83 84 85 86
C
Exon 3a
Block I
Block II
D
Exon 3c
Block I
Block II
E
Exon 3a
Thr77
Glu85
Thr78
Ser80
(Back view)
Lys83
Ser80
Ile82
TM2–TM3 linker
F
Exon 3c
Ser78
Glu86
Lys79
Lys84
Asp81
Asp81
(Back view)
Tyr83
TM2–TM3 linker

Figure 4